A Wireless Differential Protection System for Air-Core Inductors

D. Richard Brown, III, *Member, IEEE*, Jeremy A. Slater, and Alexander E. Emanuel, *Fellow, IEEE*

***Abstract*—This paper describes a new wireless differential protection system for detection of turn-to-turn faults in air-core inductors. The proposed system is composed of a pair of floating magnetic field sensors placed at opposite ends of an air-core inductor, which wirelessly communicate their measurements to a remote receiver. The receiver compares the magnetic field measurements from the sensors and triggers an alarm or circuit interruption system if the mean-squared field difference exceeds a specified threshold. The main contributions of this paper are a description of a specific realization of this differential air-core inductor protection system with several novel features and experimental results that demonstrate the sensitivity and latency of the proposed protection system. Our results suggest that deployment of the proposed system in shunt-connected inductors could help to prevent catastrophic damage resulting from turn-to-turn faults by detecting and arresting these faults in their incipient stages.**

***Index Terms*—Communication systems, inductors, protection, transformers.**

I. Introduction

DISTRIBUTED capacitance in AC transmission lines can cause the voltage at the receiving end of the transmission line to significantly exceed the voltage at the sending end of the transmission line. This phenomenon, known as the Ferranti effect, is especially pronounced in high voltage, lightly loaded, long distance AC transmission lines. If left uncompensated, overvoltages due to the Ferranti effect can cause significant damage to switchgear and equipment.

A common solution to the overvoltage problem in lightly loaded AC transmission lines is to employ shunt connected inductors directly on the high voltage (HV or EHV) transmission lines at the receiving end [1]. The construction of such HV or EHV shunt connected inductors tends to be somewhat involved and typically requires careful mechanical design, oil insulation, and cooling. Another common approach is to use shunt connected inductors on the tertiary side of a step-down transformer or autotransformer [2]. The construction of these medium voltage (MV) inductors is relatively simple by comparison where most are typically designed as dry-type simple cylindrical coils. In both cases, the purpose of the shunt connected inductor is to change the electrical characteristics of the transmission line in order to attenuate overvoltages due to the Ferranti effect in light load conditions [3], [4]. Both approaches have been proven to be effective and are widely used in practice.

A common problem characteristic for both compensation approaches is the difficulty of detecting a turn-to-turn fault in the shunt connected inductor in its incipient stage. The challenge stems from the fact that an internal fault involving a small number of turns does not increase the line current to the level needed to trip a typical overcurrent relay. While the fault currents are large enough to promote thermal damage through the inductor, the line current demand of the inductor only increases slightly during the beginning stages of the internal fault. Only when the arcing fault escalates to the point where a significant number of turns are involved can the fault be detected from the observation of the line current. At this stage, however, thermal damage to the inductor tends to be extensive, what is left from the inductor can not be salvaged, and in many circumstances collateral damage also occurs.

In the 1970s, sensor coil based protection systems were proposed as a method for detecting turn-to-turn faults in shunt connected inductors [5], [6]. These sensor coil protection systems were shown to be successful at detecting turn-to-turn faults in their incipient stages. Unfortunately, the systems described in [5], [6] required the installation of large sensing coils mounted at both ends of the inductor on solidly grounded structurals. While this design was feasible for installation on oil-filled HV and EHV shunt connected inductors, it was infeasible to install the sensor coils on the MV dry-type simple cylindrical inductors commonly used on the tertiary side of a step-down transformer or autotransformer.

This paper presents a new differential sensor coil based protection system that addresses this and several other shortcomings of the original sensor coil protection systems in [5], [6]. Specifically, our proposed *wireless* differential protection system employs a pair of small, inexpensive, floating sensors equipped with wireless digital transmitters. The floating sensors are installed at opposite ends of the dry-type cylindrical inductor but do not require any wiring or extensive structural modifications to the inductor. The transmissions from the sensors contain digitized information about the magnetic field strength at opposite ends of the inductors and are time-multiplexed so that they do not interfere with each other. A receiver, tuned to the same frequency as the transmitters, decodes the transmissions to obtain the local field measurements of the sensors. This information is then used to compute the mean-squared field difference which can be used to activate an alarm or trip signal. The main contributions of this paper are a description of a specific wireless differential protection system and a presentation of experimental results, obtained from a

Manuscript received April 7, 2004. This work was supported by Phoenix Electric Corp., Canton, MA 02021 USA. Paper no. TPWRD-00177-2004.

The authors are with the Department of Electrical and Computer Engineering, Worcester Polytechnic Institute, Worcester, MA 01609 USA (e-mail: drb@wpi.edu).

Digital Object Identifier 10.1109/TPWRD.2005.844351

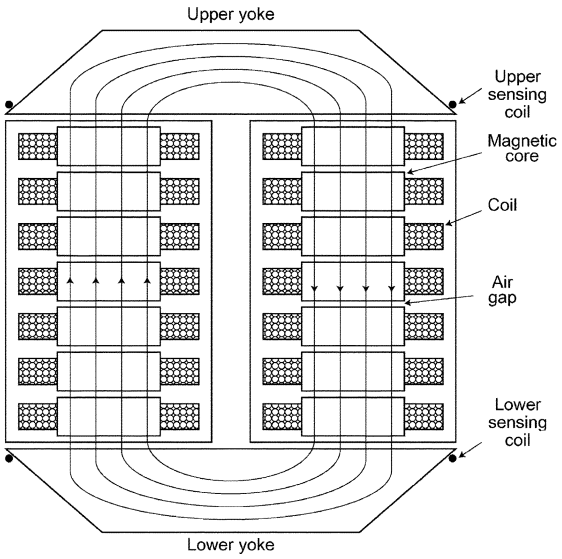

Fig. 1. Sensor coil protection system for a two-column shunt connected inductor (from [5]).

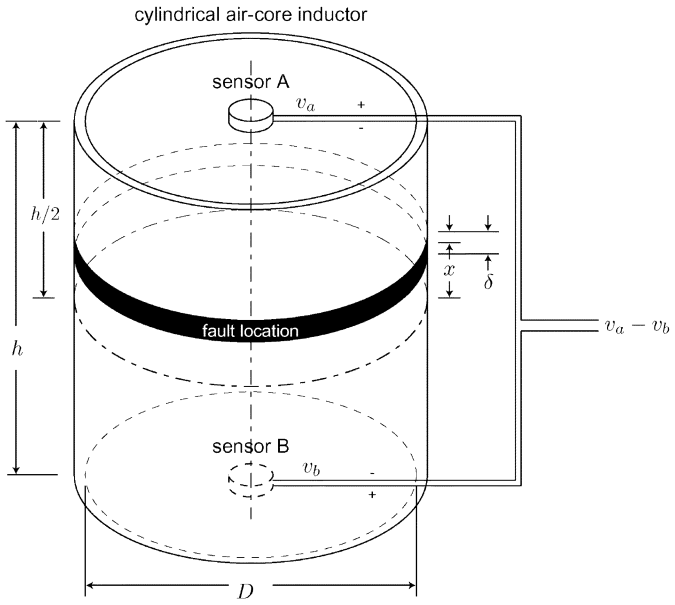

Fig. 2. Differential sensor coil protection system for a single-column cylindrical inductor.

prototype of our wireless differential protection system, that demonstrate that the proposed system is effective at quickly identifying small turn-to-turn faults in air-core inductors.

This paper is organized as follows. Section II reviews the basic concepts of differential protection and provides a theoretical analysis of the line current, faulted section current, and magnetic field differences that occur in a faulted cylindrical air-core inductor for faults of various sizes and positions. Section III describes the proposed wireless differential protection and provides a specific design example of a prototype system constructed for laboratory experimentation. Section IV presents experimental results on the sensitivity and protection latency of the wireless differential protection system using an air-core inductor, prototype sensor/transmitter pair, and prototype receiver. Finally, Section V summarizes the main contributions of our work and outlines potential areas for future research.

II. Sensor Coil Approaches for Internal Fault Protection of Shunt Reactors

Sensor coil protection schemes for shunt connected inductors are motivated by the fact that turn-to-turn faults, especially in their early stages, typically only cause small increases in the line current demand of a faulted inductor. Consequently, conventional overcurrent protection is usually inadequate for detecting this type of fault in its early stages. Sensor coil protection systems attempt to solve this problem by measuring the field disturbances, rather than the line current through the inductor, that result from a turn-to-turn fault. This section describes the basic principles of operation behind the original sensor coil protection system for shunt connected inductors described in [5] and [6] and extends these ideas to dry-type cylindrical inductors.

The original sensor coil protection system was designed to protect expensive oil-filled insulated-core inductors typically used in HV and EHV transmission systems. The first application of this idea was for a two-column inductor structure as shown in Fig. 1. In this example, a pair of identical (grounded) yokes are placed on either end of the two-column inductor structure. A sensor coil is placed around each yoke. Under normal operating conditions, the total flux entering each sensor coil is equal to the total flux leaving each sensor coil, hence the voltage induced in each sensor coil will be approximately equal to zero. When a turn-to-turn fault develops, a magnetic disturbance occurs instantaneously, the flux distribution becomes unbalanced, and the resulting sensor coil voltages will not be equal to zero. The original sensor coil protection system in [5] uses the series voltage of the sensing coils to operate a voltage actuated relay in order to quickly arrest the fault and protect the inductor from any additional thermal damage.

While the original approach in [5] was designed for a particular two-column inductor structure, the sensor coil concept can also be easily adapted to a single-column cylindrical inductor as shown in Fig. 2. In this case, the large yokes and sensor coils are replaced with a pair of relatively small, identically constructed "puck" shaped sensor coils (called sensor A and sensor B). These sensors are placed at opposite ends of the cylindrical inductor and are wired in series so that the series voltage is equal to the difference voltage $v_A - v_B$. Under normal operation, the magnetic flux linked by the sensors is approximately equal due to the symmetry of the magnetic field at the opposite ends of the inductor. Consequently, the induced voltages v_A and v_B at the output of the sensors' pick-up coils will be approximately identical and the difference voltage $v_A - v_B$ will be approximately zero. Note that, unlike the original system shown in Fig. 1, the voltages v_A and v_B in this system are not equal to zero under normal operation. The difference voltage $v_A - v_B$, however, will be approximately equal to zero. As such, we denote this system as a *differential* sensor coil protection system. When a turn-to-turn fault occurs in a noncentral $(x \neq 0)$ segment δ of the inductor, the magnetic field distribution in the interior of the inductor becomes asymmetrical. Assuming without loss of generality that the fault occurs above the midpoint of the cylindrical inductor, sensor A links a smaller magnetic flux than sensor B and the voltage difference $v_A - v_B$ becomes negative. As in the

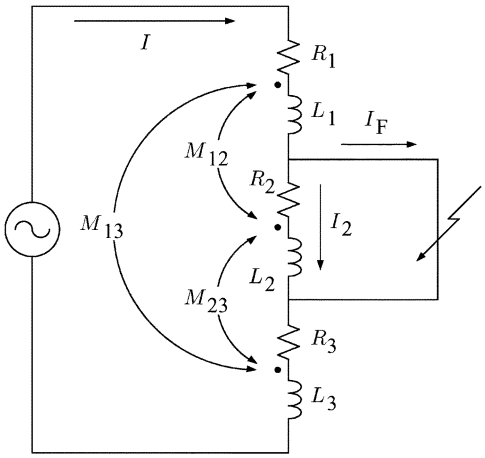

Fig. 3. Equivalent circuit of a faulted cylindrical inductor.

original system, this voltage can be used to actuate a protective relay to quickly arrest the fault.

The following sections makes the intuitive description of the differential protection system for single-column cylindrical inductors more precise. We first describe a lumped circuit model for a faulted cylindrical inductor to obtain theoretical predictions for the increase in line current that results from a turn-to-turn fault. We then derive theoretical predictions for the magnetic fields at both ends of the inductor in order to accurately describe the mechanism by which the differential protection system works.

A. Line Current Analysis of a Turn-to-Turn Faulted Cylindrical Inductor

To develop theoretical predictions for the line current through a faulted cylindrical inductor, a simple lumped circuit model for a faulted inductor is given in Fig. 3. In order to analyze this system, we first derive the governing equations for the currents and voltages in the system as a function of the resistances, inductances, and mutual inductances in the circuit. We then derive expressions for these circuit elements in terms of the physical properties of the inductor.

Under the assumption that the fault impedance is zero, the currents and voltages in the circuit shown in Fig. 3, are governed by the matrix expression

$$\begin{bmatrix} R_1+R_3+j\omega(L_1+L_3+2M_{13}) & j\omega(M_{12}+M_{23}) \\ j\omega(M_{12}+M_{23}) & R_2+j\omega L_2 \end{bmatrix} \times \begin{bmatrix} I \\ I_2 \end{bmatrix} = \begin{bmatrix} \underline{V} \\ 0 \end{bmatrix} \quad (1)$$

where $\omega = 2\pi f$, f is the frequency of the power system, $\underline{V} = V\angle 0^\circ$, and V is the rms voltage of the power system.

In order to derive expressions for the circuit elements in Fig. 3 in terms of the physical properties of the inductor, it will be convenient to establish additional notation. We define the segment lengths ℓ_i (in meters) as

$$\ell_1 = \frac{h-\delta}{2} - x \quad (2)$$

$$\ell_2 = \delta \quad (3)$$

TABLE I
DISTANCES BETWEEN ENDS OF INDUCTOR i AND j USED IN THE MUTUAL INDUCTANCE CALCULATIONS

	$i,j=1,2$	$i,j=1,3$	$i,j=2,3$
$x_1(i,j)$	$\ell_1+\ell_2$	$\ell_1+\ell_2+\ell_3$	$\ell_2+\ell_3$
$x_2(i,j)$	ℓ_2	$\ell_2+\ell_3$	ℓ_3
$x_3(i,j)$	ℓ_1	$\ell_1+\ell_2$	ℓ_2
$x_4(i,j)$	0	ℓ_2	0

and

$$\ell_3 = \frac{h-\delta}{2} + x \quad (4)$$

where h, δ, and x are defined in Fig. 2. Under our assumption that the fault occurs above the midpoint of the inductor ($x > 0$), these quantities correspond to the lengths of the shorter unfaulted segment, the faulted segment, and the longer unfaulted segment, respectively. Note that all lengths are specified in meters unless otherwise stated.

With the notation established, the resistances in (1) can be calculated as

$$R_i = \frac{\pi D N \ell_i}{h} R_0 \quad i \in \{1,2,3\} \quad (5)$$

where D is the diameter of the inductor, h is the height of the inductor, N is total number of turns, and R_0 is the nominal resistance per meter of the wire used to construct the inductor.

The self-inductances L_1, L_2, and L_3, in (1) can be calculated using standard methods for circular coils of rectangular cross section described in ([7], p. 143). This yields

$$L_i = 10^{-1}\pi^2 \left(\frac{D^2}{\ell_i}\right)\left(\frac{N\ell_i}{h}\right)^2 K_i \quad i \in \{1,2,3\} \quad (6)$$

where the units of L_i are in μH and $K_i < 1$ is Nagaoka's correction which is a function of the ratio D/ℓ_i requiring table lookup in [7].

Recognizing that the inductors L_1, L_2, and L_3 are coaxial, the mutual inductances M_{12}, M_{13}, and M_{23} can be calculated by using the standard methods described in ([7], p. 123). It is convenient to define $x_1(i,j), \ldots, x_4(i,j)$ as as the four distances between the ends of inductor i and the ends of the inductor j. Expressions for these distances are given explicitly in terms of ℓ_1, ℓ_2, and ℓ_3 in Table I.

In all three mutual inductance calculations, both inductors have the same diameter D and winding density N/h. Defining

$$r_k(i,j) = \sqrt{\left(\frac{D}{2}\right)^2 + x_k^2(i,j)} \quad (7)$$

the mutual inductances can then be written as

$$M_{ij} = 10^{-1}\left(\frac{\pi^2 D^2 N^2}{2h^2}\right) \times (r_1(i,j)B_1(i,j) - r_2(i,j)B_2(i,j) - r_3(i,j)B_3(i,j) + r_4(i,j)B_4(i,j)) \quad (8)$$

where the units of M_{ik} are in μH and $B_k(i,j)$ is a function of the ratio $D^2/r_k^2(i,j)$ requiring table lookup in [7].

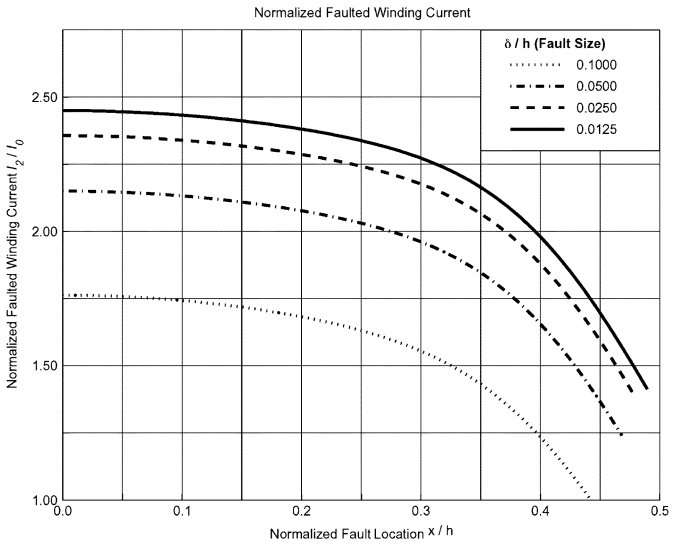

Fig. 4. Normalized current through the faulted section (I_2/I_0) of the inductor as a function of normalized fault location and normalized size of faulted section.

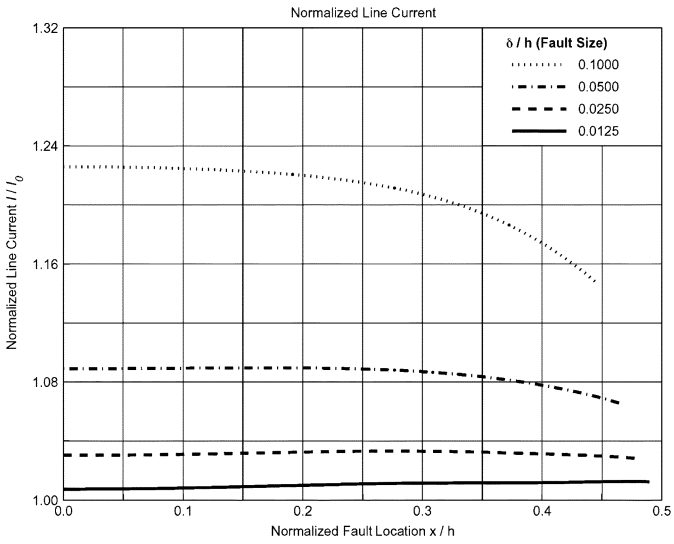

Fig. 5. Normalized line current (I/I_0) of the inductor as a function of normalized fault location and normalized size of faulted section.

Using these analytical results, Fig. 5 plots the normalized rms line current (I/I_0 where I_0 is the line current in the nonfaulted state) as a function of the normalized fault location x/h and the normalized size of the faulted section δ/h. Fig. 4 also plots the normalized rms current through the faulted section (I_2/I_0) against x/h and δ/h. The parameters used to obtain these results were $R_0 = 8.6$ mΩ/meter, $N = 333$ turns, $h = 0.9398$ meters, $D = 0.6096$ meters, and $V = 120$ volts.

The results in Fig. 4 show that turn-to-turn faults, including those that only involve a limited number of turns, can cause the current in the faulted section to increase to a point where thermal damage leads to fault propagation across the inductor. Increased current in the faulted section, however, does not cause a similar increase in the line current of the inductor. The results in Fig. 5 show that the line current through a faulted inductor does not increase significantly during the initial stages of a turn-to-turn fault, i.e., when δ/h is small. In fact, when $\delta/h < 0.05$, the normalized line current does not increase beyond $I/I_0 < 1.10$. Since this increase in line current is unlikely to be detected by an overcurrent protection system, these results motivate the development of a protection scheme that does not rely on line current to detect turn-to-turn faults. The following section shows that the field distribution at the ends of the inductor can serve as a more sensitive indicator of turn-to-turn faults in their incipient stages.

B. Field Intensity Analysis of a Turn-to-Turn Faulted Cylindrical Inductor

A current i flowing through a circular hoop of radius $D/2$ creates along the hoop's radial axis, at a distance z from the plane of the hoop, a magnetic field intensity of ([8], p. 289)

$$\boldsymbol{H}(z,i) = \frac{\frac{D^2}{4} i}{2\left(\frac{D^2}{4} + z^2\right)^{3/2}}. \tag{9}$$

This expression enables the calculation of the magnetic field intensities at the ends of the faulted cylindrical inductor as

$$\boldsymbol{H}_A = \int_0^{\ell_1} \boldsymbol{H}(z,I)\,dz + \int_{\ell_1}^{\ell_1+\ell_2} \boldsymbol{H}(z,I_2)\,dz + \int_{\ell_1+\ell_2}^{h} \boldsymbol{H}(z,I)\,dz \tag{10}$$

and

$$\boldsymbol{H}_B = \int_0^{\ell_3} \boldsymbol{H}(z,I)\,dz + \int_{\ell_3}^{\ell_2+\ell_3} \boldsymbol{H}(z,I_2)\,dz + \int_{\ell_2+\ell_3}^{h} \boldsymbol{H}(z,I)\,dz \tag{11}$$

where the segment lengths ℓ_1, ℓ_2, and ℓ_3 are defined in the previous section, I and I_2 are defined in Fig. 3, and $h = \ell_1+\ell_2+\ell_3$ is the overall height of the inductor.

The normalized differential voltage that results from the difference between the magnetic field phasors $\boldsymbol{H}_A$ and $\boldsymbol{H}_B$ is defined as

$$\Delta V = \frac{|\boldsymbol{H}_A - \boldsymbol{H}_B|}{|\boldsymbol{H}_0|} \tag{12}$$

where $\boldsymbol{H}_0$ denotes the base field intensity under normal (nonfaulted) operation when $\boldsymbol{H}_A = \boldsymbol{H}_B = \boldsymbol{H}_0$. This quantity is plotted in Fig. 6 as a function of the normalized fault location x/h and the normalized fault size δ/h.

The results in Fig. 6 demonstrate that measuring the differential field intensity is an effective method of detecting turn-to-turn faults in their early stages. This fact motivates the use of a differential protection system, rather than standard overcurrent protection, for detecting turn-to-turn faults in air-core inductors. If a turn-to-turn fault occurs at any location other than $x = 0$, the differential protection system can detect the resulting imbalance in the magnetic field intensity and quickly halt the flow of current to the inductor before more extensive thermal damage can occur. While differential protection offers several advantages over standard overcurrent protection, there are some practical limitations to the approach shown in Fig. 2 which we discuss in the following section.

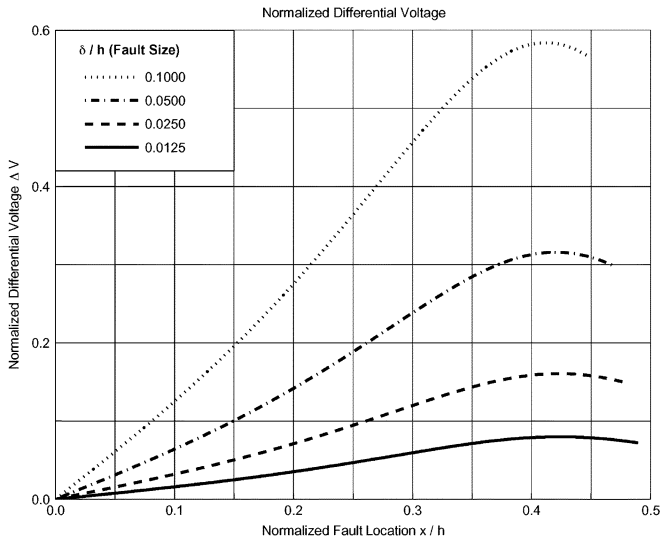

Fig. 6. Normalized differential voltage ΔV in a faulted inductor.

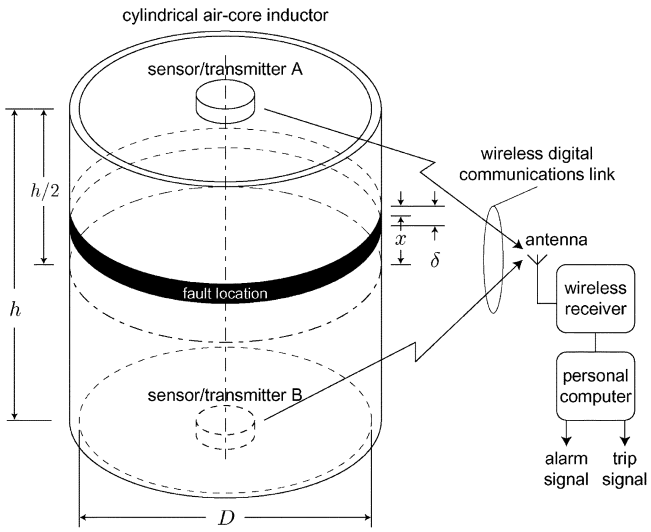

Fig. 7. Wireless differential protection system for air-core inductors.

C. Practical Limitations of the Differential Protection System

While the prior sections demonstrated that differential protection can, unlike conventional overcurrent protection, detect turn-to-turn faults in air-core inductors in their incipient stages, there are some practical limitations to the approach shown in Fig. 2. Perhaps the most significant limitation is the need to run signal wires from sensor A and sensor B to a protective relay. In most cases, the signal wires will require a ground reference which may be difficult or infeasible even in medium voltage applications. Moreover, due to the high magnetic field intensities in the vicinity of the inductor, there is potential for the signal pairs from sensor A and sensor B to be unintentionally influenced by external fields and/or noise. If the signal wires are not carefully routed and shielded, the noise picked up by these wires may cause the differential protection system to generate false alarms or trips.

The following sections describes a new *wireless* differential protection system that uses floating sensors and a wireless digital communications link to address these limitations. The basic concepts of the proposed wireless system are described first and then the details of a specific prototype implementation are presented.

III. Wireless Differential Protection System for Air-Core Inductors

In this section, we describe a wireless differential protection system that addresses the most significant practical limitations of the hardwired differential protection system described in Section II. The primary difference is that our proposed system replaces the hardwired analog link between the sensors and the protective relay with a digital wireless communications link. While the wireless communications link removes the requirements for grounding and for careful routing of the signal and common wires between the sensors (and the digital nature of the link also improves the fidelity of the field measurements), this feature poses new challenges due to the requirement for active electronics in the sensors to realize a useful wireless communications link. A key feature of the proposed system is an additional power supply coil and a voltage regulator in each sensor to provide a self-contained means for powering the sensor's electronics without batteries or external power connections. These features allow the wireless sensors to be easily installed and virtually maintenance free.

Fig. 7 shows the main features of the proposed wireless differential protection system. The proposed system relies on the same basic principle of operation as the original differential protection system shown in Fig. 2, but allows for a simpler installation and improved safety, accuracy, and flexibility with respect to the original approach.

A prototype of the system shown in Fig. 7 was constructed using off-the-shelf electronic components. The balance of this section describes the specific details of a prototype wireless differential protection system built to verify the efficacy of the proposed approach and used to obtain the experimental results presented in Section IV. While the design presented in this section is not unique, we present it here as a tangible demonstration of our approach and also to describe several specific design choices that we believe result in a highly practical and useful system.

A. Sensors/Transmitters

A block diagram of the wireless sensor/transmitter developed for the wireless differential protection system prototype is shown in Fig. 8. An important feature of the sensor/transmitter is that the same device is used in both sensor positions (A and B) with no configuration other than the orientation of the sensor (sensor B must be inverted with respect to sensor A). Moreover, the sensor/transmitter design is fully self-contained, maintenance-free, and could be completely potted in epoxy, if desired, without any loss of functionality. The details of the sensor/transmitter prototype are described in the following subsections.

1) Sensor/Transmitter Power Supply: The wireless sensor/transmitter requires at least a simple power supply to drive the active components in the circuit. While it is possible achieve this by directly connecting AC power to the sensor, this approach

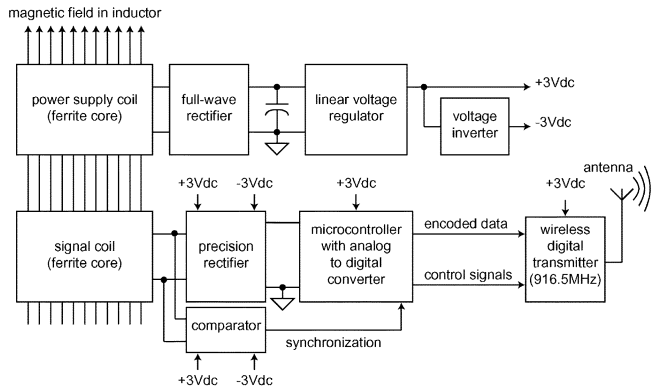

Fig. 8. Block diagram of wireless sensor/transmitter.

would increase the installation costs and significantly reduce the advantage of using a wireless communication link. A battery-powered sensor/transmitter is also undesirable due to the inconvenience of periodic battery replacement. The approach used here is to supply power to the active components in the sensor/transmitter by scavenging power directly from the inductor's magnetic field.

A simple power supply was constructed as follows. A power supply coil (separate from the signal coil) with a ferrite core was built as an integral component of the sensor/transmitter with its output connected to a full-wave rectifier made of General Semiconductor 1N5817 rectifier Schottky diodes. The output of the rectifier is filtered by a 330 μF electrolytic capacitor. To produce the stable ± 3 Vdc signals required for accurate signal conditioning and analog to digital conversion, a Texas Instruments TPS77030DBVT 3 V 50 mA low-drop-out linear voltage regulator and a MAXIM MAX665 voltage inverter are used. The output specifications of the power supply vary depending on the field intensity of the air-core inductor in which it is installed, but this power supply was more than adequate to meet the requirements of the sensor/transmitter in the small prototype inductor described in Section IV.

2) Sensor/Transmitter Signal Path: The sensor/transmitter in the wireless differential protection system uses a signal coil with a ferrite core to acquire an induced voltage signal proportional to the magnetic flux density at one end of the inductor. Unlike the system in Fig. 2, however, the wireless differential protection system's sensor/transmitter performs several local operations on the measured signal before communicating this signal to the decision-making components of the protection system. This section describes the details of our approach to the design of a simple sensor/transmitter signal path.

In our design, the signal coil generates an induced AC voltage waveform proportional to the magnetic flux density at one end of the inductor. Since the differential protection algorithm does not need to know the polarity of the measured signal, the AC voltage waveform from the signal coil is rectified with a precision rectifier composed of a pair of Texas Instruments OPA4342PA op-amps, four General Semiconductor 1N5817 Schottky diodes and several 1% tolerance resistors. The precision rectifier circuit also includes a gain control to prevent undesirable clipping in the op-amps while also maximizing use of the dynamic range of the analog to digital converter (ADC).

A PIC12F675 microcontroller with a built in ADC is used to sample the rectified signal coil waveform and to digitize the samples for the remaining processing. The ADC in the microcontroller is programmed to sample the waveform at 480 Hz with each sample providing 10 bits of resolution. A 16 bit cyclic redundancy check (CRC) [9] is calculated and updated as each sample is obtained. After the final sample of each period is acquired the CRC calculation completes. When the synchronization pulse is received from the comparator, the microcontroller dynamically Manchester encodes and simultaneously sends the data to the 916.5 MHz wireless digital transmitter. Specific details of the communication protocol are discussed in Section III-B.

The 916.5 MHz wireless digital transmitter used in our sensor/transmitter is an RF Monolithics TR1100 amplitude shift keyed (ASK) transceiver. While the TR1100 contains both a transmitter and receiver, the system is designed to operate with a unidirectional communication link and the receiver is not used by the sensor/transmitter. The TR1100 has very low power consumption and meets all FCC requirements for unlicensed transmission in the 900 MHz band. The antenna, chosen for its small size and good performance, is a surface mount Linx Technologies Splatch antenna.

All electronics in the sensor/transmitter were chosen for low power consumption to allow the sensor/transmitter to work effectively in a low field intensity environment. Experimental results with a prototype sensor showed that the electronics in the sensor/transmitter signal path draw, on average, approximately 7 mA on the $+3$ Vdc rail and 4 mA on the -3 Vdc rail.

B. Communication Protocol and Synchronization

An important part of the overall wireless differential protection system is the design of an efficient and reliable communication protocol between the sensor/transmitter and receiver. This section describes the basics of the custom communication protocol used in our prototype wireless differential protection system.

The TR1100 ASK transmitter is configured to transmit data at a rate of 150 kbits per second. Recall that the sensor/transmitter samples the precision rectifier output at a rate of 480 Hz. Rather than transmitting the measured data continuously (which would be power-inefficient as well as require the two transmitters to operate at different frequencies or use a code division multiple access scheme to avoid mutual interference), the data over one period of the power cycle is buffered by the microcontroller and sent as a short burst transmission at the start of the following period. The TR1100 transmitter remains in an off state except during this burst transmission interval at the start of each period.

To compute the total time required for the burst transmission, recall that each ADC sample contains 10 bits. Hence, the sensor/transmitter generates 80 bits of measurement data in each 60 Hz power cycle. To maximize efficiency, these bits are packed into 10 bytes of data called the payload. The payload is prepended by one synchronization byte to aid timing recovery of the Manchester encoded signal at the receiver and appended by one phase identifier byte and two CRC bytes to allow the receiver to detect errors in the payload. Additionally, each byte includes a start and stop bit. The total packet length is thus equal

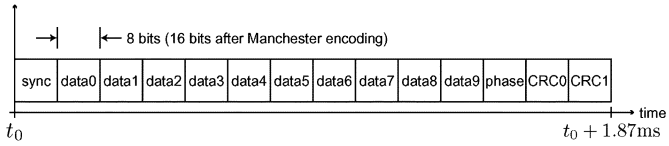

Fig. 9. Data packet sent once per period per sensor/transmitter.

to 14 bytes and is shown in Fig. 9. Conversion to the Manchester encoded format (required by the TR1100 transceiver) results in a total of 28 bytes (280 total bits including start and stop bits) to be transmitted once per period of the 60 Hz power system. The total burst transmission thus requires approximately 1.87 ms at the TR1100 s transmit rate of 150 kbits per second.

Since the sensor/transmitters are identical and operating autonomously, it is important to provide a mechanism in the communication protocol to ensure that the transmissions of different sensors do not temporally overlap and cause a loss of data due to mutual interference. There are several possible solutions to this problem with varying degrees of complexity. An elegant and simple solution to this problem is to synchronize the transmissions to occur at positive-slope zero-crossings of the waveform at the output of the signal coil. Applied directly, this approach causes both sensor/transmitters to transmit at exactly the same time, which is undesirable, but inverting one sensor causes the positive-slope zero-crossing of sensor A to occur 180 degrees out of phase from sensor B. Consequently, the burst transmissions of a sensor pair (with one sensor inverted) occur approximately 8.3 ms apart. This provides a more than adequate guard time between successive transmissions to avoid interference even in a severe multipath channel.

We note that the sensor/transmitter transmission times are short enough to allow deployment of the wireless differential protection system in a three-phase 60 Hz power system. Such a system would require three pairs of sensor/transmitters but only one receiver and one personal computer to protect three inductors. Assuming that one sensor of each pair is inverted, the sensors will all automatically synchronize to unique 2.8 ms timeslots in the 60 Hz period. In this case, guard times between successive transmissions remain approximately 1 ms. Although we have not tested this configuration, our analysis suggests that the system has sufficient margins to ensure that mutual interference will be automatically avoided in three-phase power systems. Moreover, the sensor/transmitter and protocol design is universal and can be applied in single- or three-phase systems without modification.

C. Wireless Receiver

A custom receiver was also designed for the wireless differential protection system as an interface between the wireless data and the PC. A block diagram of this receiver is shown in Fig. 10.

The receiver uses an identical Splatch antenna and TR1100 transceiver as the sensor/transmitter to receive and demodulate the incoming ASK data. In this case, the transmitter function of the TR1100 transceiver is not used. The Manchester encoded data at the output of the TR1100 transceiver is sent to the custom programmed ALTERA MAX EPM9320LC84-20 CPLD for decoding, frame synchronization, and time stamping. The CPLD output is then sent to a DLP-USB232 M USB-Serial UART interface module to allow for high-speed communications with the PC through a standard universal serial bus (USB) port. We note that the maximum throughput of the DLP-USB232 M is 3 Mbits per second, which exceeds the throughput requirements of the overall wireless differential system. To simplify the design, we also considered directly interfacing to the PC via a standard serial RS-232 port, but this option was ruled out due to the fact that the throughput of most PC RS-232 serial ports does not meet the requirements.

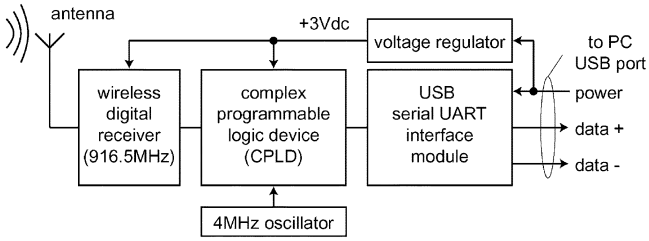

Fig. 10. Receiver block diagram.

D. Differential Protection Software

The final component of the wireless differential protection system is the PC running a custom software package that reads data from the wireless receiver (through the USB port) and provides the user with powerful real-time analysis as well as an intuitive and informative graphical user interface.

A simple Windows-based test application was written to verify the operation of the wireless differential protection system. Key features of the software included a pair of signal strength meters to show the status of the wireless links, an oscilloscope-style display of one period of the 60 Hz waveform received from each sensor/transmitter and the calculated difference between the waveforms, and a user selectable alarm threshold.

The software computes the mean-squared difference (MSD) between the two waveforms each time a new valid data packet is received from either transmitter. Denote the most recent 8-sample data packet as $\boldsymbol{x}_0 = [x_0(1), \ldots, x_0(8)]$ where $x_0(1)$ is the oldest sample and the $x_0(8)$ is the most recent sample in the packet. The packet received one half cycle before the $\boldsymbol{x}_0$ packet is denoted as $\boldsymbol{x}_{-1}$ and the packet received a full cycle before the $\boldsymbol{x}_0$ packet is denoted as $\boldsymbol{x}_{-2}$. Note that packets $\boldsymbol{x}_0$ and $\boldsymbol{x}_{-2}$ are received from the same sensor/transmitter and packet $\boldsymbol{x}_{-1}$ is received from the opposite sensor/transmitter. When packet $\boldsymbol{x}_0$ has been received, the mean-squared difference is computed as

$$\text{MSD} = \frac{1}{8}\left[\sum_{n=1}^{4}(x_{-1}(n) - x_{-2}(n+4))^2 + \sum_{n=5}^{8}(x_{-1}(n) - x_0(n-4))^2\right]. \quad (13)$$

In a single-phase 60 Hz power system, packets arrive every 8.33 ms and the MSD is computed 120 times per second. The differential protection software allows the user to manually set alarm and trip thresholds. When the MSD exceeds these thresholds, the software signals that a fault has been detected by activating one or more logic-level outputs in the PC's parallel port.

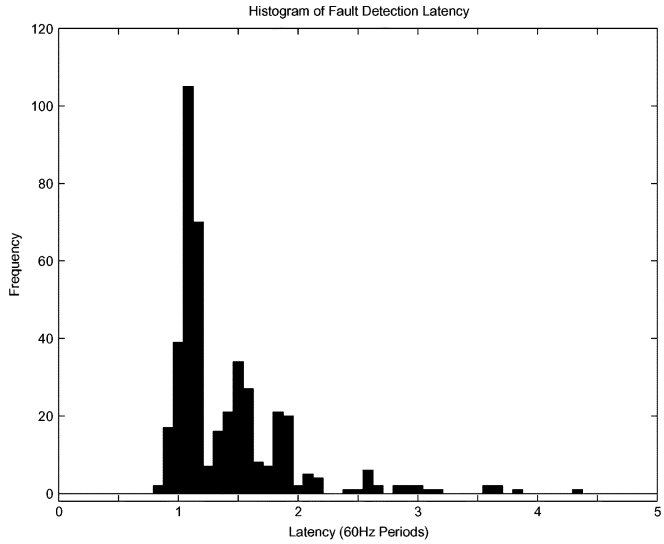

Fig. 11. Histogram of experimental fault detection latency results.

This signal can be used by a protective relay to arrest the fault and remove the faulted coil from the power system.

IV. Experimental Results

An air-core cylindrical inductor was constructed for testing purposes from 333 turns of 14 awg wire with a diameter of 24 inches and a height of 37 inches. This reactor draws approximately 8 amps when plugged directly into a 120 V wall outlet and produces a large enough magnetic field to power the wireless sensor/transmitters. Small segments of insulation were removed from multiple turns on the top half of the inductor to facilitate simulation of turn-to-turn faults by shorting the turns with a small segment of 14 awg wire. Experiments with this inductor showed that the proposed wireless differential protection system was able to detect turn-to-turn faults as small as five turns $(\delta/x \approx 0.015)$ at all positions except the midpoint of the inductor $(x = 0)$.

The most important characteristic of this protection system is that it detects faults quickly and accurately. Experimental results show that the proposed wireless differential protection system detects faults within a few cycles of the 60 Hz power system. It was necessary to use external equipment to measure the time difference between a fault and its detection due to the speed of detection. Using an analysis system, including a logic analyzer and an oscilloscope, test data was acquired from the PC parallel port and from a current clamp around the shorting wire. The analyzer was configured to trigger on the rising edge of the parallel port data pin and capture a 100 ms history of analog data from the current clamp. From this analog data, the latency of a single test is the time between when the AC signal appears on the current clamp and the time when rising edge appears on the PC's parallel port. Fig. 11 shows a histogram of the fault detection latency of approximately 500 experiments. Note that the experiments were not synchronized to the 60 Hz power system.

Fig. 11 shows that a majority of faults are detected within two 60 Hz periods. There is a 8.33 ms periodicity in the latency since a new transmission packet arrives and the MSD is computed every half cycle. The peaks in the histogram occur at these 8.33 ms locations because a fault is most likely to be detected if there is an entire half cycle of faulted field measurements in the buffer. The quickest detections occur after roughly one cycle, while even the slowest detections occur in less than five cycles. All of the detections that occur past the second cycle have been determined to be due solely to bit errors in the wireless transmissions. The results in Fig. 11 suggest that, in the absence of bit errors, the maximum latency of the proposed wireless differential protection system is approximately 33 ms.

V. Conclusion

This paper describes a new differential sensor coil protection scheme that can be applied directly to cylindrical air-core inductors commonly used for overvoltage compensation in lightly loaded AC transmission systems. The proposed wireless differential protection system addresses many of the shortcomings of the original hardwired sensor coil protection systems while retaining the essential sensitivity of the sensor coil approach. The proposed system can be constructed of inexpensive, off-the-shelf electronic components, is relatively easy to install, uses unlicensed frequencies, and is essentially maintenance free. Experimental results demonstrate that the proposed system is able to detect turn-to-turn faults in their incipient stages and can issue a trip signal to a protective relay within a few cycles of detection.

To avoid false alarms and trips, the prototype system presented in this paper used a communication protocol that specified a CRC checksum in each packet from each sensor. This checksum allowed for the detection of bit errors in the packet, but did not facilitate correction of these errors. More sophisticated channel coding in the sensors would allow for both detection and correction of errors in the receiver. Future prototypes of this system would likely benefit from some form of channel coding to reduce the likelihood of communication errors, improve the range, increase the reliability, and reduce the overall latency of the proposed wireless differential protection system.

Acknowledgment

The authors would like to thank D. Feinzeig for his help building the inductor and the prototype wireless differential protection system as well as his help in proofreading the manuscript.

References

[1] M. Christoffel, "The design and testing of EHV shunt reactors," *IEEE Trans. Power App. Syst.*, vol. PAS-86, pp. 684–692, Jun. 1967.
[2] G. Sheble, *Reactive Power: Basics, Problems, and Solutions*. Piscataway, NJ: IEEE Tutorial Course, 1987.
[3] J. Miller, *Reactive Power Control in Electric Systems*. New York, NY: Wiley, 1982.
[4] G. Jancke, R. Jenkins, B. Nordstrom, and L. Norlin, "The choice of shunt reactors for the swedish 400 kV system," in *Proc. CIGRE*, 1962, Report 412.
[5] J. Vora and A. Emanuel, "Senor coil for internal fault protection of shunt reactors," *IEEE Trans. Power App. Syst.*, vol. PAS-93, pp. 1917–1926, Nov./Dec. 1974.
[6] A. Emanuel, "Transformer internal fault detector using leakage field changes," in *IEEE PES Winter Meeting*, vol. C74, New York, NY, Jan. 1974, pp. 240–248.
[7] F. Grover, *Inductance Calculations*. New York: Van Nostrant, 1946.
[8] M. Sadiku, *Elements of Electromagnetics*. New York: HRV Sounders College Publishing, 1989.

[9] S. Wicker, *Error Control Systems for Digital Communication and Storage*. Upper Saddle River, NJ: Prentice Hall, 1995.

D. Richard Brown, III (SM'97–M'00) received the B.S. and M.S. degrees in electrical engineering from the University of Connecticut, Storrs, in 1992 and 1996, respectively, and the Ph.D. degree in electrical engineering with a minor in mathematics from Cornell University, Ithaca, NY, in 2000.

From 1992 to 1997, he was a Development Engineer and Project Manager with General Electric Company, Plainville, CT. Since 2000, he has been an Assistant Professor with the Department of Electrical and Computer Engineering, Worcester Polytechnic Institute, Worcester, MA. His research interests include multiuser communication systems, cooperative networks, and adaptive signal processing.

Jeremy A. Slater received the B.S. degree in electrical engineering from Worcester Polytechnic Institute, Worcester, MA, in 2004. He is currently pursuing the M.S. degree at Worcester Polytechnic Institute.

His current research involves nondestructive evaluation for the detection of oxides within cast aluminum.

Alexander E. Emanuel (SM'70–F'98) received the B.Sc., M.Sc., and D.Sc. degree with Technion, Israel Institute of Technology.

Currently, he is a Professor of Electrical and Computer Engineering at Worcester Polytechnic Institute (WPI), Worcester, MA. He has been a member of the faculty since 1974. He began to study electrical engineering at the Bucharest Polytechnic Institute. In 1969, he joined High Voltage Engineering where he participated in high voltage equipment R&D. His research interest is power quality and power electronics.